

RESEARCH ARTICLE | JUNE 17 2024

Quantum motion of oxygen and hydrogen in water: Atomic and total kinetic energy across melting from neutron scattering measurements

Special Collection: [Water: Molecular Origins of its Anomalies](#)






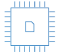
Giovanni Romanelli   ; Carla Andreani  ; Alessio Bocedi  ; Roberto Senesi 



J. Chem. Phys. 160, 234503 (2024)


<https://doi.org/10.1063/5.0211165>



 Nanotechnology & Materials Science  Optics & Photonics  Impedance Analysis  Scanning Probe Microscopy  Sensors  Failure Analysis & Semiconductors

Unlock the Full Spectrum.
From DC to 8.5 GHz.
Your Application. Measured.

[Find out more](#)



Quantum motion of oxygen and hydrogen in water: Atomic and total kinetic energy across melting from neutron scattering measurements

Cite as: J. Chem. Phys. 160, 234503 (2024); doi: 10.1063/5.0211165

Submitted: 29 March 2024 • Accepted: 22 May 2024 •

Published Online: 17 June 2024



View Online



Export Citation



CrossMark

Giovanni Romanelli,^{1,a)}  Carla Andreani,^{1,b)}  Alessio Bocedi,²  and Roberto Senesi^{1,c)} 

AFFILIATIONS

¹ Dipartimento di Fisica and NAST Centre, Università degli Studi di Roma "Tor Vergata," via della Ricerca Scientifica 1, 00133 Rome, Italy

² Dipartimento di Scienze e Tecnologie Chimiche and NAST Centre, Università degli Studi di Roma "Tor Vergata," via della Ricerca Scientifica 1, 00133 Rome, Italy

Note: This paper is part of the JCP Special Topic on Water: Molecular Origins of its Anomalies.

^{a)} **Also at:** ISIS Neutron and Muon Source, Rutherford Appleton Laboratory, Chilton OX110QX, United Kingdom.

Author to whom correspondence should be addressed: giovanni.romanelli@uniroma2.it

^{b)} **Also at:** National Research Council, Institute of Polymers, Composites and Biomaterials (IPCB), Naples, Italy.

^{c)} **Also at:** National Research Council, Istituto di Struttura della Materia (ISM), Rome, Italy.

ABSTRACT

We provide a concurrent measurement of the hydrogen and oxygen nuclear kinetic energies in the water molecule across melting at 270 K in the solid phase and 276 K in the liquid phase. Experimental values are obtained by analyzing the neutron Compton profiles of each atomic species in a deep inelastic neutron scattering experiment. The concurrent measurement of the atom kinetic energy of both hydrogen and oxygen allows the estimate of the total kinetic energy per molecule due to the motion of nuclei, specifically 35.3 ± 0.8 and 34.8 ± 0.8 kJ/mol for the solid and liquid phases, respectively. Such a small difference supports results from *ab initio* simulations and phenomenological models from the literature on the mechanism of competing quantum effects across the phase change. Despite the experimental uncertainties, the results are consistent with the trend from state-of-the-art computer simulations, whereby the atom and molecule kinetic energies in the liquid phase would be slightly lower than in the solid phase. Moreover, the small change of nuclear kinetic energy across melting can be used to simplify the calculation of neutron-related environmental dose in complex locations, such as high altitude or polar neutron radiation research stations where liquid water and ice are both present: for neutron energies between hundreds of meV and tens of keV, the total scattering cross section per molecule in the two phases can be considered the same, with the macroscopic cross section only depending upon the density changes of water near the melting point.

© 2024 Author(s). All article content, except where otherwise noted, is licensed under a Creative Commons Attribution-NonCommercial-NoDerivs 4.0 International (CC BY-NC-ND) license (<https://creativecommons.org/licenses/by-nc-nd/4.0/>). <https://doi.org/10.1063/5.0211165>

I. INTRODUCTION

Quantum effects in water and water-related systems affect the properties of their condensed phases at the microscopic to macroscopic scales in isotope-specific ways. For this reason, a number of investigations have concentrated on the quantum effects on the lightest atom, hydrogen, in a number of materials. Over the past two decades, the topic has greatly benefited from joint approaches (see, e.g., Refs. 1–3) based on Deep Inelastic Neutron Scattering

and non-classical computer simulations, such as semi-empirical models, or computer simulations based on Density Functional Theory or Path-Integral Molecular Dynamics (PIMD). These experimental and theoretical techniques can assess the kinetic energies of nuclei in molecular systems, which can be considered a thermometer of the magnitude of nuclear quantum effects, which have deep consequences, e.g., on biochemical reactions^{4,5} and imply changes in nominal isotope concentrations depending on physical and chemical variables.^{6,7}

Among many molecular systems, water represents a particularly fascinating example. Beyond the importance of water for biology and life, deviations from the classical (non-quantum) dynamics of hydrogen and oxygen impact the modeling of neutron transport simulations for radiation protection, dose calculation, and the development of new neutron moderators at state-of-the-art neutron sources.^{8–11} Environmental radiation levels are affected by secondary neutrons, created by cosmic rays interacting with the atmosphere, whose energy spectrum is modified by moderation processes at ground levels.^{12,13} In such cases, the dose calculation related to fast and thermal neutrons in complex environments depends upon soil moisture and snow cover at mountain altitudes¹⁴ or at high-altitude Antarctic plateaus.¹⁵ In this context, the detailed knowledge of nuclear quantum effects in water just above and below the melting point can make radiation dose calculations more accurate in complex environments where ice and liquid water may coexist.

Despite the amount of published literature studying hydrogen dynamics, values for the kinetic energy [Nuclear Kinetic Energy (NKE)] of oxygen in water, either experimental or theoretical, are much less available. Ramirez and Herrero¹⁶ reported the value of the oxygen NKE from Path Integral Molecular Dynamics (PIMD), simulations of water in the gas, liquid, and solid phases as 48.5, 52.3, and 52.8 meV, respectively. Lin *et al.*,¹⁷ through an anisotropic quasi-harmonic phonon calculation of open path integral Car-Parrinello molecular dynamics data for ice Ih at 269 K, estimated an oxygen kinetic energy of 56.4 meV. Ceriotti and Manolopoulos, performing imaginary-time PIMD with a carefully designed generalized Langevin equation, reported values of 54.6 meV and 58.1 for oxygen in H₂O and D₂O at 300 K, respectively,¹⁸ while Pinilla *et al.*,⁷ using PIMD approaches, obtained values of the oxygen NKE at the triple point of 52.7 and 52.4 meV for ice and liquid water, respectively. The first experimental values for the oxygen NKE in heavy water across melting¹⁹ provided values in the liquid and solid phases that were different by less than 1 meV (about 1.5% of the total), also supported by PIMD simulations. The relatively small difference (1 meV), despite the drastic changes in vibrational energies (about 12 meV shift for librations and 14 meV for stretching, in opposite directions²⁰) and structure across the melting, was explained by a cancellation mechanism described as competing quantum effects. The mechanism of competing quantum effects was qualitatively explained in analogy to a two-level quantum system with an environment-dependent off-diagonal coupling, playing the role of hydrogen bonding. A phase transition, provoking a small change in the coupling, shifts the eigenvalues of the system by the same amount but in opposite directions.¹⁹ Upon melting, librations undergo a red-shift, while stretching increases in frequency. In a harmonic picture where the NKE can be evaluated through the average vibrational frequency weighted by the vibrational density of states, these shifts approximately cancel out.

The small difference in the oxygen NKE, $\langle E_K \rangle_O$, across melting was discussed in Ref. 16 using PIMD and suggested a slightly lower value in the liquid phase than in the solid, which was reflected also on the hydrogen kinetic energy, $\langle E_K \rangle_H$, and on the total kinetic energy per molecule, K . Similarly, using a semi-empirical method combining discrete molecular vibrations, librations, and translations in water, Finkelstein and Moreh²¹ showed an approximate continuity in the kinetic energy of both hydrogen and oxygen over a wide temperature range encompassing the liquid and solid forms. Pinilla

*et al.*⁷ calculated both hydrogen and oxygen NKEs, reporting very similar values across melting, again with that in the solid phase being slightly higher than in the liquid for both nuclei. Larger differences in the oxygen NKE are expected and measured upon H-D substitution due to the reduced mass effect, as reported by Vos *et al.*²² for Ice Ih and its deuterated counterpart at a fixed temperature of 118 K using electron scattering at high momentum transfer.

Here, we provide the concurrent experimental determination of the NKEs of hydrogen and oxygen in liquid water and ice across melting using DINS. Combining the values from each nucleus in the molecule, we also provide the total nuclear kinetic energy per molecule, which can be directly compared with PIMD simulations from the literature.

II. EXPERIMENTAL

The DINS technique,^{1,23} also referred to as Neutron Compton Scattering (NCS), allows mass-selective spectroscopy experiments with neutrons, whereby the signals from isotopes with different

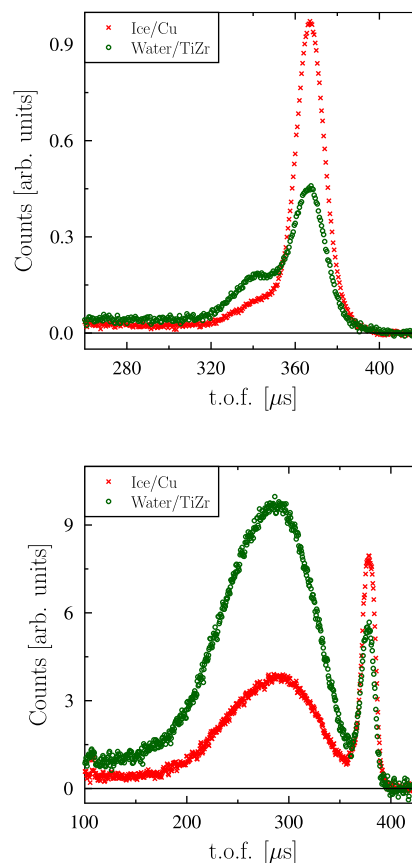


FIG. 1. Raw time-of-flight spectra for ice in a copper container at 270 K (red crosses) and liquid water in a titanium-zirconium container at 276 K (green circles). The top panel corresponds to the sum of all backward scattering detectors, while the bottom panel corresponds to the sum of signals from forward-scattering detectors from 142 to 170 (scattering angles between 35° and 60°).

masses are treated independently owing to the Impulse Approximation (IA).^{24–26} Within the IA, the neutron scattering intensity is centered at the atomic recoil energy, whereas the dynamic structure factor $S(Q, \omega)$ can be expressed as the linear superposition of a Neutron Compton Profile (NCP), $J(y)$, from each isotope j in a sample

$$S_{IA}(Q, \omega) = \sum_j I_j \frac{M_j}{\hbar Q} J(y_j), \quad (1)$$

where $\hbar\omega$ and Q are the neutron energy and wavevector transfer during the scattering process, I_j is a weighting factor considering the stoichiometry and bound scattering cross section of isotope j , M_j is the mass of the struck atom and,

$$y_j = \frac{M_j}{\hbar^2 Q} \left(\hbar\omega - \frac{\hbar^2 Q^2}{2M_j} \right) \quad (2)$$

is the isotope-specific West scaling variable.²⁷ The dependence of the West scaling variable upon isotope mass allows the separation of the neutron scattering intensity into mass-separated isotope-specific

peaks. The NCP is related to the nuclear momentum distribution, a probability density function measuring the momentum spread of a particle due to its spatial localization in a potential. The second moment of the nuclear momentum distribution is proportional to the nuclear kinetic energy of an atom which, for a light-weight quantum particle in a confining potential, is substantially higher than the classical prediction from a Maxwell–Boltzmann theory of a gas of non-interacting particles, namely $3k_B T/2$, where k_B is the Boltzmann constant and T is the thermodynamic temperature of the system.

DINS experiments were performed at the VESUVIO spectrometer^{28,29} at the ISIS Neutron and Muon Source (UK).³⁰ Two containers were used: a copper container, already used in Ref. 19, for the solid sample, and a TiZr container for the liquid sample. The containers were placed within the instrument's closed circuit refrigerator and equipped with heaters for temperature control. The flat-faced containers were positioned with the large face perpendicular to the incident neutron beam, allowing the use of both front-scattering and back-scattering detectors on the instrument. In order to measure the energy transfer, the neutron energy of scattered neutrons was fixed using the 4.9 eV neutron capture resonance in ¹⁹⁷Au foils at room temperature, while the neutron energy before the scattering event was calculated using the

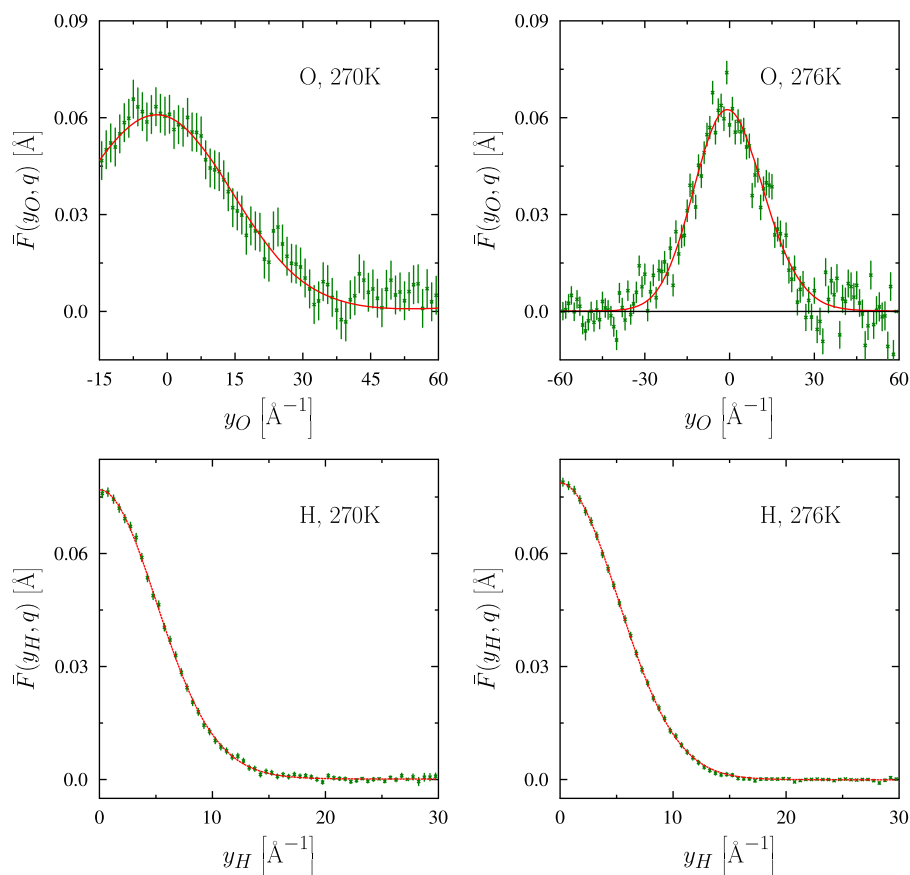


FIG. 2. The corrected oxygen (top) and hydrogen (bottom) NCPs in ice at 270 K (left) and in liquid water at 276 K (right). Experimental data are reported as circles with error bars, and the best fit as red solid lines.

time-of-flight (t.o.f.) technique. DINS spectra for forward-scattering and back-scattering detectors were obtained using the foil-cycling³¹ and double-difference³² techniques, respectively. Examples of spectra from banks of detectors in the t.o.f. domain are reported in Fig. 1. In particular, the top panel reports back-scattering spectra featuring the signal from oxygen (left peak) partially isolated from the signal due to the container (right peak). On the other hand, the bottom panel, corresponding to front-scattering detectors, features a large signal due to neutron scattering from hydrogen (left peak) and an additional signal (right composite peak) corresponding to the overlap of NCPs from oxygen and the elements composing the container. The intensity and position of the peak from the container play a crucial role in the analysis of the oxygen NCP. Copper, used for the solid sample, has a bound scattering cross section of 8.03 b, while titanium and zirconium have bound scattering cross sections of 4.35 and 6.36 b, respectively.³³ The higher scattering power of the copper container compared to the TiZr one can be easily appreciated in its higher relative intensity compared to the signal from water (hydrogen in forward scattering and oxygen in backward scattering, i.e., top and bottom panels in Fig. 1). However, while less intense, the composite peak of the TiZr container has an increased overlap with the oxygen NCP compared to copper, with titanium having a lower atomic mass than copper.

DINS spectra were analyzed separately for the forward and backward scattering detectors in order to isolate the hydrogen and oxygen NCPs, respectively. In both cases, the data were corrected for the multiple scattering contribution using a Monte Carlo approach,³⁴ and the forward scattering detectors were corrected for the sample-dependent gamma background.³¹ The entire data reduction process followed the procedure described in Ref. 35.

III. RESULTS AND DISCUSSION

Figure 2 shows the oxygen (top) and hydrogen (bottom) NCPs in their West-scaling domains from ice at 270 K (left) and liquid water at 276 K. In particular, we report the experimental Compton profiles, $\bar{F}(y, Q)$, corresponding to the sum over all backward scattering (oxygen) and forward scattering (hydrogen) detectors. Moreover, as the hydrogen NCP is symmetrized as a final step of the data correction,³⁵ only the data for $y_H \geq 0 \text{ \AA}^{-1}$ are reported. The best fit using a Gauss–Hermite model,³⁷ including the convolution, for each detector, with the experimental resolution,³⁶ is also reported for both nuclei as a red solid line. For oxygen (both liquid and ice) and for hydrogen in the liquid form, the Gauss–Hermite expansion was truncated at the leading Gaussian term, while for hydrogen in ice, the first Hermite polynomial ($n = 4$) was also used, confirming the higher anisotropy of the hydrogen momentum distribution in the solid phase than in the liquid one.³⁸ In the case of the oxygen NCP, we report in the figure the y_O range where the data were analyzed. The fitted values of the NCP width, expressed as the average NKE of hydrogen and oxygen, are reported in Table I together with other values reported in the literature. It is worth noting that the assessment of nuclear and total kinetic energies is approached by different authors in several ways and, consequently, using different units of measurement (meV, kJ/mol, and kcal/mol). In order to facilitate the comparison of our results with the theoretical values already published, we have adopted in each comparison the units used in the reference theoretical work. A conversion rule to change from one unit to another is as follows:

$$1 \text{ kcal/mol} \simeq 43.4 \text{ meV} \simeq 4.18 \text{ kJ/mol} \quad (3)$$

From the experimental point of view, the concurrent measurement of hydrogen and oxygen in a DINS experiment is a complex

TABLE I. Values of the total nuclear kinetic energy of hydrogen and oxygen in H₂O and deuterium and oxygen in D₂O for liquid water and ice at temperatures near the melting point. The value of the total kinetic energy per molecule, K , is also reported.

H ₂ O	Phase	T (K)	$\langle E_K \rangle_H$ (meV)	$\langle E_K \rangle_O$ (meV)	K (kJ/mol)	Reference
DINS	Ice Ih	270	157 ± 2	52 ± 5	35.3 ± 0.8	a
INS	Ice Ih	271	153.7 ± 2	20
DINS	Ice Ih	271	157 ± 2	39
PIMD/NN	Ice	273	155.5	52.7	35.1	40
PIMD/NN	Liquid	273	154.7	52.5	34.9	40
DINS	Liquid	276	155 ± 2	51 ± 5	34.8 ± 0.8	a
INS	Liquid	276	152 ± 2	41
SE	Liquid	276	154	21
DINS	Liquid	300	146 ± 3	39
D ₂ O	Phase	T (K)	$\langle E_K \rangle_D$ (meV)	$\langle E_K \rangle_O$ (meV)	K (kJ/mol)	Reference
DINS	Ice Ih	274	108 ± 2	60 ± 4	26.6 ± 0.8	19
PIMD	Ice Ih	274	108.3	55.7	26.3	19
DINS	Liquid	280	112 ± 2	61 ± 3	27.5 ± 0.8	19
PIMD	Liquid	280	108.7	55.6	26.3	19

^aPresent work.

task because of the large difference in their scattering cross sections, by a factor of almost 20. In fact, the double-differential scattering cross section in a DINS experiment is weighted, in the incoherent approximation, by the total bound scattering cross sections that, for hydrogen and oxygen, are 82.03 and 4.232 b, respectively.³³ The high scattering cross section of hydrogen requires only small amounts of samples in order to obtain a good statistics in a DINS experiment. On the other hand, larger quantities of samples are requested to measure the oxygen NCP. However, larger samples also imply larger contributions from multiple scatterings, which increase the complexity of its analysis. For this reason, the concurrent measurement of D and O in heavy water, where the difference in scattering cross sections is less than 2, was already achieved a decade ago.¹⁹ By comparing the top and bottom panels of Fig. 2, one can appreciate how, for a given quantity of sample, there is a marked difference in the quality of the experimental data, with the error bars in the hydrogen NCP much smaller than those in the oxygen one.

The experimental values for the oxygen NKE are in excellent agreement with those previously reported in Ref. 7 (see Fig. 3) and with those from Ref. 40 (see Table I), although the 0.2 meV difference predicted by the PIMD/NN simulations is too subtle to be observed in the experimental data. Our data also confirm the predictions from semi-empirical models,²¹ which imply a mild dependence of the kinetic energy on the phase change. The semi-empirical model is based on the assumption that within the harmonic approximation, the NKE can be predicted as half of the total energy related to a set of harmonic oscillators representing internal vibrations (discrete in nature) and external and lattice modes which, for water clusters linked by hydrogen bonding, correspond to hindered translations and librational modes. In this framework, and by assuming a discrete vibrational density of states, one has^{3,21,42,43}

$$\langle E_K \rangle_O = \sum_{\alpha} f_{\alpha} \frac{\hbar\omega_{\alpha}}{4} \coth\left(\frac{\hbar\omega_{\alpha}}{2k_B T}\right), \quad (4)$$

where the summation runs over the discrete vibrations, both internal (stretching and bending) and external (translations and librations), each with a frequency ω_{α} . The parameters f_{α} describe the energy uptake of oxygen from each harmonic oscillation. As hydrogen has the lowest mass in the molecule, it takes most of the energy from the internal vibrations, and the same is true for librational modes, as oxygen is near the molecule's center of mass or axes of rotation. Of the parameters f_{α} , the one corresponding to translations is the largest, as it is defined by the ratio of the oxygen mass to the mass of the molecule, $f_i = M_O/(2M_H + M_O)$, and it needs to be considered three times for each spatial dimension. The second consideration has to do with the separation in energy of the different modes: internal modes are found at several hundreds of meV, libration modes in the range 70–80 meV, and translation modes at about 20–30 meV (see, e.g., Refs. 20, 21, and 42). In the temperature range around the melting point of water, the internal modes only occupy the vibrational ground state, so they are just contributing with a zero-point energy (ZPE) constant term, while the contribution from low-lying translational modes can be approximated as the one from free translations (knowing that $\coth(x) \rightarrow 1/x$ as $x \rightarrow 0$). Librational modes are in an intermediate regime because of the partial occupation of the first excited state. However, considering the overall contribution

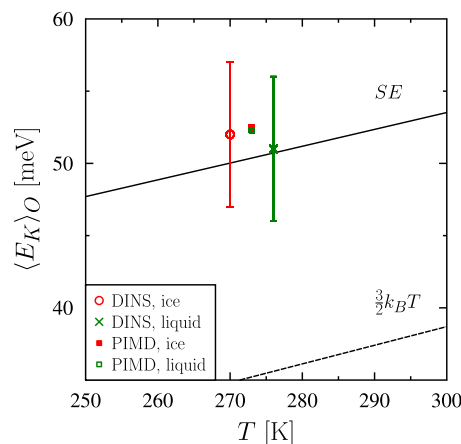


FIG. 3. Experimental oxygen NKE in light water across the melting point in the solid (red circle) and liquid (green cross). The results from PIMD simulations in Ref. 7 for ice and liquid water at 273 K are reported as filled red and empty green squares, respectively. The prediction from the semi-empirical (SE) harmonic model is reported as a solid black line, and the Maxwell–Boltzmann classical prediction is reported as a dashed black line.

of librations to the oxygen NKE (with $f_{\alpha} \approx 5\%$) being about 3 meV out of about 50 meV, one can approximate the previous equation as

$$\langle E_K \rangle_O \approx \frac{3}{2} f_i k_B T + \text{ZPE}. \quad (5)$$

In this context, it was noted²¹ how the temperature dependence of oxygen NKE was affected very little by the phase change, although it implied a change in the definition of both f_{α} and ω_{α} . This is true because the competing quantum effects effectively cancel out the ZPE contribution in Eq. (5). The approximately linear dependence of $\langle E_K \rangle_O$ on T can be appreciated in Fig. 3 by comparison with the classical Maxwell–Boltzmann prediction: the semi-empirical model provides a NKE increased by about 15 meV compared to the classical limit, with a slope slightly decreased by a factor f_i .

The concurrent measurement of both the hydrogen and oxygen NKEs allowed the estimation of the total kinetic energy per molecule, K , which is sometimes reported in the literature.^{16,44} Figure 4 shows the experimental values from DINS as compared with the results from PIMD simulations in Ref. 40, obtained by combining the provided values of $\langle E_K \rangle_H$ and $\langle E_K \rangle_O$, namely

$$K = 2\langle E_K \rangle_H + \langle E_K \rangle_O, \quad (6)$$

for ice and liquid water at 273 K. When looking at the total kinetic energy, the small difference between the ice (larger) and liquid (smaller) values becomes more apparent, as both hydrogen and oxygen NKEs decrease upon melting according to the PIMD simulations, both from Refs. 40 and 16. The experimental results in Fig. 4 seem to suggest the same trend, although the difference is comparable to the experimental uncertainties. While the agreement with the results from Ref. 40 extends on the absolute scale, the values from Ref. 16 are lower by about 1 kJ/mol (about 3%).

A similar small discrepancy in the total kinetic energy in the case of solid H₂O can be appreciated in Fig. 5, where the DINS data

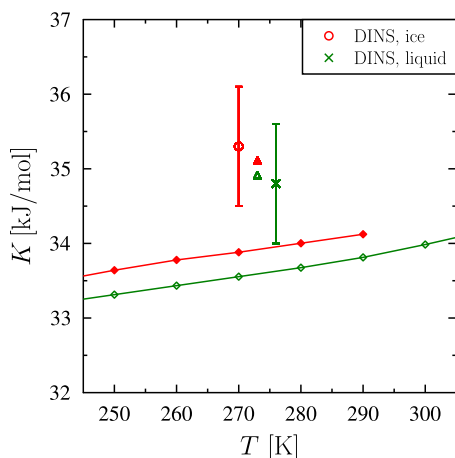


FIG. 4. Experimental total kinetic energy in light water across the melting point in the solid (red circle) and liquid (green cross). The results from PIMD simulations in Ref. 40 ($K = 2(\langle E_K \rangle_H + \langle E_K \rangle_O)$) for ice and liquid water at 273 K are reported as filled and empty red triangles, respectively. Finally, the temperature dependencies of K for ice and liquid water from Ref. 16 are reported as filled red and empty green diamonds.

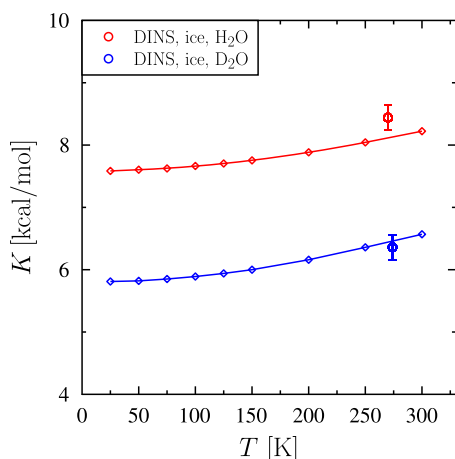


FIG. 5. The total kinetic energy per molecule obtained from DINS experiments for light ice (this work) and heavy ice (Ref. 19) are reported as red and blue circles with error bars. They are compared with the results from PIMD simulations from Ref. 44 for light ice (red diamonds) and heavy ice (blue diamonds).

from ice at 270 K are compared with the results from PIMD simulations from Ref. 44. In the same reference, isotope nuclear quantum effects were discussed by calculating the value of K for heavy ice as well, which is reported in Fig. 5 and compared with the corresponding experimental value of K from Ref. 19 (using the values of $\langle E_K \rangle_D$ and $\langle E_K \rangle_O$ reported in Table I). As opposed to the slight difference in the case of light ice, in the case of heavy ice, the experimental data are in good agreement, within the experimental uncertainties, with the results from Ref. 16.

Finally, the values of the NKE for hydrogen and oxygen can be used to approximate the energy-dependent total scattering cross sections at hot-to-epithermal neutron energies. This can be performed in the formalism of the Short-Collision Time (SCT)⁴⁵ approximation, whereby the neutron scattering from free nuclei is corrected by an effective temperature related to the NKE ($3k_B T_{eff,j}/2 = \langle E_K \rangle$). The scattering cross section for each element becomes

$$\sigma_j(E) = \sigma_{b,j} \left(\frac{A_j}{A_j + 1} \right)^2 \left(1 + \frac{k_B T_{eff,j}}{2A_j E} \right), \quad (7)$$

with E the incident neutron energy and A_j the atomic mass number in units of the neutron mass, $\sigma_{b,j}$ its bound scattering cross section.³³ We note here the difference between the bound scattering cross section, a constant parameter not dependent upon the neutron energy and related to the neutron scattering length, and the total scattering cross section, $\sigma(E)$, the result of the integration of the dynamic structure factor (or the double-differential scattering cross section) over all scattering angles and final energies of the neutron, which is a function of the incident neutron energy. The total scattering cross section of the molecule is—under the same assumptions of Eq. (1),

$$\sigma(E) = \sum_j N_j \sigma_j(E) \approx \sum_j N_j \sigma_{f,j}, \quad (8)$$

where N_j represents the stoichiometry of the molecule, and $\sigma_{f,j} = \sigma_{b,j} A_j^2 / (A_j + 1)^2$ is the constant free-scattering cross-section parameter. The right-hand side of Eq. (8) only holds for energies above a few eV. The ability of Eq. (8) to reproduce the experimental data can be appreciated in Fig. 6, where the SCT approximation is exemplified in the case of ice at 270 K, using the DINS parameters obtained in this study to evaluate the effective temperatures affecting hydrogen and oxygen. The experimental data, collected on VESUVIO concurrently with the DINS measurement and making use of the capabilities for neutron transmission measurements,⁴⁶ can be approximated by the SCT already at a few hundreds of meV, where one could expect more structured contributions from stretching modes in the multi-phonon-expansion approximation to the total scattering cross section.^{47,48} A similar agreement in the same energy range was also found for hydrogenated alcohols.⁴⁹ As the NKEs for both oxygen and hydrogen across melting are found to be the same within the experimental error bars, one can safely assume that the total scattering cross section per molecule of liquid water and ice across melting can be considered equal, with the macroscopic cross section (i.e., the microscopic cross section multiplied by the number density of scattering centers) only affected by the temperature- and phase-dependent variations in the bulk density. It is also worth noting that the hydrogen NKE of pure light water across melting, presented here, is more similar in value to that of seawater at high pressure than to that of room-temperature water at ambient pressure.⁵⁰ These findings are relevant in the context of neutron transport modeling of the thermal scattering law in applications ranging from environmental field-scale soil moisture analysis for the quantification of biomass and snow^{51,52} to investigations of neutron albedo in space weather ground-level and altitude observations,^{53,54} where water hydrogen in soil, air, liquid water, and snow determines the amount of ground albedo neutrons in the sensitive energy ranges.

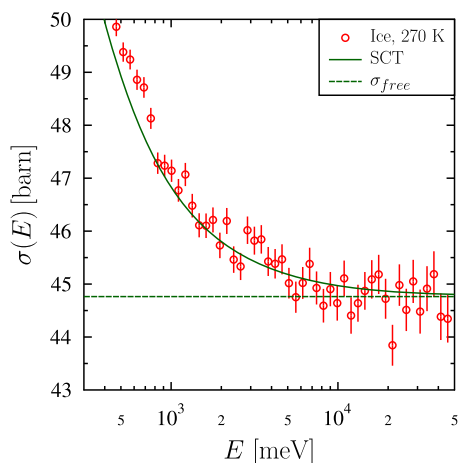


FIG. 6. Experimental total cross section per water molecule (red markers and error bars) compared with the short collision time prediction (green line).

IV. CONCLUSION

We have provided a concurrent experimental determination of the oxygen and hydrogen nuclear kinetic energies in water across melting in the ice and liquid water phases at 270 and 276 K, respectively. The experimental results support the idea of competing quantum effects, which leave the average kinetic energy of each nucleus in the water molecule approximately unchanged. Qualitatively, our experimental results are consistent with the slight decrease of hydrogen, oxygen, and total kinetic energies going from the solid to the liquid phase, as reported by state-of-the-art computer simulations.

The concurrent determination of both oxygen and hydrogen average nuclear kinetic energies allows us to provide a consistent approximation to the total scattering cross section of liquid water and ice between hundreds of meV and a few keV, using the short collision time approximation. Such simplification can be used to improve estimates of the fraction of ground albedo neutrons in environmental models and the resulting relevance of neutron attenuation during particle transport mechanisms⁵⁵ in complex settings where liquid water and ice coexist across saturated atmospheric layers and mixed water/snow areas, such as high-altitude mountains⁵⁶ and polar^{54,57} research stations.

ACKNOWLEDGMENTS

The authors gratefully acknowledge the support of the ISIS@MACH ITALIA Research Infrastructure, the hub of ISIS Neutron and Muon Source (UK), (MUR official registry No. U. 0008642.28-05-2020—April 16, 2020). The financial support from the Consiglio Nazionale delle Ricerche within the CNR-STFC Grant Agreement (No. 2021-2027) concerning collaboration in scientific research at the ISIS (UK) of STFC is gratefully acknowledged. The STFC Rutherford Appleton Laboratory is acknowledged for its access to neutron beam facilities.

AUTHOR DECLARATIONS

Conflict of Interest

The authors have no conflicts to disclose.

Author Contributions

Giovanni Romanelli: Formal analysis (equal); Investigation (equal); Methodology (equal); Writing – original draft (equal). **Carla Andreani:** Conceptualization (equal); Investigation (equal); Writing – review & editing (equal). **Alessio Bocedi:** Conceptualization (equal); Investigation (equal); Writing – review & editing (equal). **Roberto Senesi:** Conceptualization (equal); Formal analysis (equal); Investigation (equal); Writing – original draft (equal).

DATA AVAILABILITY

The data that support the findings of this study are available from the corresponding author upon reasonable request.

REFERENCES

- C. Andreani, D. Colognesi, J. Mayers, G. F. Reiter, and R. Senesi, “Measurement of momentum distribution of lightatoms and molecules in condensed matter systems using inelastic neutron scattering,” *Adv. Phys.* **54**, 377–469 (2005).
- M. Ceriotti, W. Fang, P. G. Kusalik, R. H. McKenzie, A. Michaelides, M. A. Morales, and T. E. Markland, “Nuclear quantum effects in water and aqueous systems: Experiment, theory, and current challenges,” *Chem. Rev.* **116**, 7529–7550 (2016).
- R. Moreh, W. C. Selley, D. Sutton, and R. Vodhanel, “Widths of the 6.92 and 7.12 MeV levels in ¹⁶O and the influence of the effective temperature,” *Phys. Rev. C* **31**, 2314–2316 (1985).
- R. K. Allemann and N. S. Scrutton, *Quantum Tunnelling in Enzyme-Catalysed Reactions* (Royal Society of Chemistry, 2009).
- G. R. Fleming, G. D. Scholes, and Y.-C. Cheng, “Quantum effects in biology,” *Procedia Chem.* **3**, 38–57 (2011), 22nd Solvay Conference on Chemistry.
- T. E. Markland and B. Berne, “Unraveling quantum mechanical effects in water using isotopic fractionation,” *Proc. Natl. Acad. Sci. U. S. A.* **109**, 7988–7991 (2012).
- C. Pinilla, M. Blanchard, E. Balan, G. Ferlat, R. Vuilleumier, and F. Mauri, “Equilibrium fractionation of H and O isotopes in water from path integral molecular dynamics,” *Geochim. Cosmochim. Acta* **135**, 203–216 (2014).
- A. Viñales, J. Dawidowski, and J. Márquez Damián, “Neutron total cross-section model for liquids and its application to light water,” *Ann. Nucl. Energy* **38**, 1687–1692 (2011).
- M. Martellucci, G. Romanelli, S. Valeri, D. Cottone, C. Andreani, and R. Senesi, “The neutron cross section of barite-enriched concrete for radioprotection shielding in the range 1 meV–1 keV,” *Eur. Phys. J. Plus* **136**, 259 (2021).
- G. Noguere, J. P. Scotta, S. Xu, E. Farhi, J. Ollivier, Y. Calzavara, S. Rols, M. Koza, and J. I. Marquez Damian, “Temperature-dependent dynamic structure factors for liquid water inferred from inelastic neutron scattering measurements,” *J. Chem. Phys.* **155**, 024502 (2021).
- J. I. Marquez Damian, J. Dawidowski, R. J. Granada, F. Cantargi, G. Romanelli, C. Helman, M. Krzystyniak, G. Skoro, D. Roubtsov, and D. Roubtsov, “Experimental validation of the temperature behavior of the ENDF/B-VIII.0 thermal scattering kernel for light water,” *EPJ Web Conf.* **239**, 14001 (2020).
- L. Dorman, *Cosmic Rays in the Earth’s Atmosphere and Underground* (Springer Science & Business Media, 2013), Vol. 303.
- M. Eisenbud and T. F. Gesell, *Environmental Radioactivity from Natural, Industrial and Military Sources: From Natural, Industrial and Military Sources* (Elsevier, 1997).

- ¹⁴T. Brall, V. Mares, R. Bütikofer, and W. Rühm, "Assessment of neutrons from secondary cosmic rays at mountain altitudes—Geant4 simulations of environmental parameters including soil moisture and snow cover," *Cryosphere* **15**, 4769–4780 (2021).
- ¹⁵A. Mishev, S. Kodaira, H. Kitamura, O. Ploc, I. Ambrožová, R. Toloček, I. Kartsev, V. Shurshakov, A. Artamonov, and K. Inozemtsev, "Radiation environment in high-altitude antarctic plateau: Recent measurements and model studies," *Sci. Total Environ.* **890**, 164304 (2023).
- ¹⁶R. Ramirez and C. P. Herrero, "Kinetic energy of protons in ice Ih and water: A path integral study," *Phys. Rev. B* **84**, 064130 (2011).
- ¹⁷L. Lin, J. A. Morrone, R. Car, and M. Parrinello, "Momentum distribution, vibrational dynamics, and the potential of mean force in ice," *Phys. Rev. B* **83**, 220302 (2011).
- ¹⁸M. Ceriotti and D. E. Manolopoulos, "Efficient first-principles calculation of the quantum kinetic energy and momentum distribution of nuclei," *Phys. Rev. Lett.* **109**, 100604 (2012).
- ¹⁹G. Romanelli, M. Ceriotti, D. E. Manolopoulos, C. Pantalei, R. Senesi, and C. Andreani, "Direct measurement of competing quantum effects on the kinetic energy of heavy water upon melting," *J. Phys. Chem. Lett.* **4**, 3251–3256 (2013).
- ²⁰C. Andreani, G. Romanelli, and R. Senesi, "A combined INS and DINS study of proton quantum dynamics of ice and water across the triple point and in the supercritical phase," *Chem. Phys.* **427**, 106–110 (2013).
- ²¹Y. Finkelstein and R. Moreh, "Temperature dependence of the proton kinetic energy in water between 5 and 673K," *Chem. Phys.* **431–432**, 58–63 (2014).
- ²²M. Vos, E. Weigold, and R. Moreh, "Elastic electron scattering from water vapor and ice at high momentum transfer," *J. Chem. Phys.* **138**, 044307 (2013).
- ²³C. Andreani, M. Krzystyniak, G. Romanelli, R. Senesi, and F. Fernandez-Alonso, "Electron-volt neutron spectroscopy: Beyond fundamental systems," *Adv. Phys.* **66**, 1–73 (2017).
- ²⁴G. K. Ivanov and Y. S. Sayasov, "Theory of the vibrational excitation of a molecule in the impulse approximation," *Sov. Phys.-Dokl.* **9**, 171 (1964).
- ²⁵V. Sears, "Slow-neutron multiple scattering," *Adv. Phys.* **24**, 1–45 (1975).
- ²⁶H. A. Gersch, L. J. Rodriguez, and P. N. Smith, "Corrections to the impulse approximation for high-energy neutron scattering from liquid helium," *Phys. Rev. A* **5**, 1547–1558 (1972).
- ²⁷G. B. West, "Electron scattering from atoms, nuclei and nucleons," *Phys. Rep.* **18**, 263–323 (1975).
- ²⁸J. Mayers and G. Reiter, "The vesuvio electron volt neutron spectrometer," *Meas. Sci. Technol.* **23**, 045902 (2012).
- ²⁹G. Romanelli, M. Krzystyniak, R. Senesi, D. Raspino, J. Boxall, D. Pooley, S. Moorby, E. Schooneveld, N. J. Rhodes, C. Andreani, and F. Fernandez-Alonso, "Characterisation of the incident beam and current diffraction capabilities on the vesuvio spectrometer," *Meas. Sci. Technol.* **28**, 095501 (2017).
- ³⁰See <http://www.isis.stfc.ac.uk> for information about the ISIS Pulsed Neutron and Muon Source (last accessed on May 2024).
- ³¹E. M. Schooneveld, J. Mayers, N. J. Rhodes, A. Pietropaolo, C. Andreani, R. Senesi, G. Gorini, E. Perelli-Cippo, and M. Tardocchi, "Foil cycling technique for the VESUVIO spectrometer operating in the resonance detector configuration," *Rev. Sci. Instrum.* **77**, 5103 (2006).
- ³²C. Andreani, D. Colognesi, E. Degiorgi, A. Filabozzi, M. Nardone, E. Pace, A. Pietropaolo, and R. Senesi, "Double difference method in deep inelastic neutron scattering on the VESUVIO spectrometer," *Nucl. Instrum. Methods Phys. Res., Sect. A* **497**, 535–549 (2003).
- ³³V. F. Sears, "Neutron scattering lengths and cross sections," *Neutron News* **3**, 26–37 (1992).
- ³⁴J. Mayers, A. L. Fielding, and R. Senesi, *Nucl. Instrum. Methods Phys. Res., Sect. A* **481**, 454 (2002).
- ³⁵G. Romanelli, B. Hewer, M. Krzystyniak, M. Gigg, R. Tolchenov, S. Mukhopadhyay, and F. Fernandez-Alonso, "Data analysis of neutron Compton scattering experiments using MANTID," *J. Phys.: Conf. Ser.* **1055**, 012016 (2018).
- ³⁶G. Romanelli and M. Krzystyniak, "On the line-shape analysis of Compton profiles and its application to neutron scattering," *Nucl. Instrum. Methods Phys. Res., Sect. A* **819**, 84–88 (2016).
- ³⁷S. Imberti, C. Andreani, V. Garbuio, G. Gorini, A. Pietropaolo, R. Senesi, and M. Tardocchi, "Resolution of the VESUVIO spectrometer for high-energy inelastic neutron scattering experiments," *Nucl. Instrum. Methods Phys. Res., Sect. A* **552**, 463 (2005).
- ³⁸C. Andreani, R. Senesi, M. Krzystyniak, G. Romanelli, and F. Fernandez-Alonso, "Experimental studies of nuclear quantum effects in condensed matter: The case of water," *Riv. Nuovo Cimento* **41**, 291–340 (2018).
- ³⁹C. Andreani, G. Romanelli, and R. Senesi, "Direct measurements of quantum kinetic energy tensor in stable and metastable water near the triple point: An experimental benchmark," *J. Phys. Chem. Lett.* **7**, 2216–2220 (2016).
- ⁴⁰B. Cheng, J. Behler, and M. Ceriotti, "Nuclear quantum effects in water at the triple point: Using theory as a link between experiments," *J. Phys. Chem. Lett.* **7**, 2210–2215 (2016).
- ⁴¹R. Senesi, D. Flammini, A. I. Kolesnikov, E. D. Murray, G. Galli, and C. Andreani, "The quantum nature of the OH stretching mode in ice and water probed by neutron scattering experiments," *J. Chem. Phys.* **139**, 074504 (2013).
- ⁴²G. Romanelli, F. Fernandez-Alonso, and C. Andreani, "The harmonic picture of nuclear mean kinetic energies in heavy water," *J. Phys.: Conf. Ser.* **571**, 012003 (2014).
- ⁴³P. Ulpiani, G. Romanelli, D. Onorati, M. Krzystyniak, C. Andreani, and R. Senesi, "The effective isotropy of the hydrogen local potential in biphenyl and other hydrocarbons," *J. Chem. Phys.* **153**, 234306 (2020).
- ⁴⁴C. P. Herrero and R. Ramirez, "Isotope effects in ice Ih: A path-integral simulation," *J. Chem. Phys.* **134**, 094510 (2011), arXiv:1108.1923 [cond-mat.mtrl-sci].
- ⁴⁵H. McMurry, I. U. National Reactor Testing Station, and P. P. C. A. E. Division, "Differential scattering cross sections of moderators in the short collision time approximation: Theoretical," in AEC Research and Development Report No. Pt. 1 (U.S. Atomic Energy Commission, Idaho Operations Office, 1962).
- ⁴⁶J. Robledo, J. Dawidowski, J. M. Damián, G. Škoro, C. Bovo, and G. Romanelli, "Measurement of neutron total cross sections at the vesuvio spectrometer," *Nucl. Instrum. Methods Phys. Res., Sect. A* **971**, 164096 (2020).
- ⁴⁷A. Sjolander, "Multi-phonon processes in slow neutron scattering by crystals," *Ark. Fys.* **14**, 1 (1958).
- ⁴⁸G. Romanelli, D. Onorati, P. Ulpiani, S. Cancelli, E. Perelli-Cippo, J. I. Márquez Damián, S. C. Capelli, G. Croci, A. Muraro, M. Tardocchi *et al.*, "Thermal neutron cross sections of amino acids from average contributions of functional groups," *J. Phys.: Condens. Matter* **33**, 285901 (2021).
- ⁴⁹J. Dawidowski, L. Rodríguez Palomino, G. Romanelli, G. Cuello, J. Márquez Damián, J. Robledo, and M. Krzystyniak, "Determination of effective temperatures of hydrogenated and deuterated alcohols using the vesuvio spectrometer," *Nucl. Instrum. Methods Phys. Res., Sect. A* **989**, 164948 (2021).
- ⁵⁰A. Bocedi, G. Romanelli, C. Andreani, and R. Senesi, "Hydrogen nuclear mean kinetic energy in water down the Mariana Trench: Competition of pressure and salinity," *J. Chem. Phys.* **153**, 134306 (2020).
- ⁵¹J. Jakobi, J. A. Huisman, M. Köhli, D. Rasche, H. Vereecken, and H. R. Bogen, "The footprint characteristics of cosmic ray thermal neutrons," *Geophys. Res. Lett.* **48**, e2021GL094281, <https://doi.org/10.1029/2021gl094281> (2021).
- ⁵²M. Köhli, M. Schrön, S. Zacharias, and U. Schmidt, "Uranos v1.0—The ultra rapid adaptable neutron-only simulation for environmental research," *Geosci. Model Dev.* **16**, 449–477 (2023).
- ⁵³C. Weulersse, M. Mazurek, C. D. Pinas, R. Mills, and B. Guerard, "Thermal neutron measurements inside an aircraft for sea assessment," *IEEE Trans. Nucl. Sci.* **70**, 1548–1554 (2023).
- ⁵⁴G. Hubert, "Analyses of continuous measurements of cosmic ray induced-neutrons spectra at the concordia antarctic station from 2016 to 2024," *Astropart. Phys.* **159**, 102949 (2024).
- ⁵⁵R. Baatz, H. R. Bogen, H.-J. Hendricks Franssen, J. A. Huisman, C. Montzka, and H. Vereecken, "An empirical vegetation correction for soil water content quantification using cosmic ray probes," *Water Resour. Res.* **51**, 2030–2046, <https://doi.org/10.1002/2014wr016443> (2015).

⁵⁶S. Vernetto, M. Laurenza, M. Storini, A. Zanini, P. Diego, S. Massetti, A. Libertore, J. Terrazas, C. Vigorito, P. Vallania, and S. Cirilli, "Long term measurements of neutron dose rates at Testa Grigia high altitude research station (3480 m. a.s.l.)," *Radiat. Phys. Chem.* **193**, 109972 (2022).

⁵⁷J. D. Wille, S. P. Alexander, C. Amory, R. Baiman, L. Barthélemy, D. M. Bergstrom, A. Berne, H. Binder, J. Blanchet, D. Bozkurt, T. J. Bracegirdle, M. Casado, T. Choi, K. R. Clem, F. Codron, R. Datta, S. D. Battista, V. Favier, D.

Francis, A. D. Fraser, E. Fourré, R. D. Garreaud, C. Genthon, I. V. Gorodetskaya, S. González-Herrero, V. J. Heinrich, G. Hubert, H. Joos, S.-J. Kim, J. C. King, C. Kittel, A. Landais, M. Lazzara, G. H. Leonard, J. L. Lieser, M. MacLennan, D. Mikolajczyk, P. Neff, I. Ollivier, G. Picard, B. Pohl, F. M. Ralph, P. Rowe, E. Schlosser, C. A. Shields, I. J. Smith, M. Sprenger, L. Trusel, D. Udy, T. Vance, É. Vignon, C. Walker, N. Wever, and X. Zou, "The extraordinary march 2022 East Antarctica "heat" wave. Part II: Impacts on the Antarctic ice sheet," *J. Clim.* **37**, 779–799 (2024).